

**Dieses Dokument ist eine Zweitveröffentlichung (Verlagsversion) /
This is a self-archiving document (published version):**

Alexander Hammer, Matthieu Scherpf, Martin Schmidt, Hannes Ernst, Hagen Malberg,
Klaus Matschke, Adrian Dragu, Judy Martin, Olimpiu Bota

Camera-based assessment of cutaneous perfusion strength in a clinical setting

Erstveröffentlichung in / First published in:

Physiological Measurement. 2022, 43 (2), Art. Nr. 025007 [Zugriff am: 26.08.2022]. IOPScience.
ISSN 0967-3334.

DOI: <http://doi.org/10.1088/1361-6579/ac557d>

Diese Version ist verfügbar / This version is available on:

<https://nbn-resolving.org/urn:nbn:de:bsz:14-qucosa2-805056>



Dieses Werk ist lizenziert unter einer [Creative Commons Namensnennung 4.0 International Lizenz](https://creativecommons.org/licenses/by/4.0/).

This work is licensed under a [Creative Commons Attribution 4.0 International License](https://creativecommons.org/licenses/by/4.0/).



PAPER

Camera-based assessment of cutaneous perfusion strength in a clinical setting

OPEN ACCESS

RECEIVED

3 November 2021

REVISED

1 February 2022

ACCEPTED FOR PUBLICATION

15 February 2022



PUBLISHED

21 March 2022

Original content from this work may be used under the terms of the [Creative Commons Attribution 4.0 licence](https://creativecommons.org/licenses/by/4.0/).

Any further distribution of this work must maintain attribution to the author(s) and the title of the work, journal citation and DOI.



Alexander Hammer^{1,4} , Matthieu Scherpf¹ , Martin Schmidt¹ , Hannes Ernst¹ , Hagen Malberg¹, Klaus Matschke², Adrian Dragu³ , Judy Martin³  and Olimpiu Bota³ 

¹ Institute of Biomedical Engineering, TU Dresden, Dresden, Germany

² Department of Cardiac Surgery, University Heart Center Dresden, TU Dresden, Dresden, Germany

³ University Center for Orthopedics, Trauma, and Plastic Surgery, Faculty of Medicine Carl Gustav Carus, TU Dresden, Dresden, Germany

⁴ Present address: Institute of Biomedical Engineering, TU Dresden, Fetscherstr. 29, 01307 Dresden, Germany.

E-mail: alexander.hammer@tu-dresden.de

Keywords: camera-based photoplethysmography, remote measurement, non-contact, perfusion strength, skin flap transplants

Abstract

Objective. After skin flap transplants, perfusion strength monitoring is essential for the early detection of tissue perfusion disorders and thus to ensure the survival of skin flaps. Camera-based photoplethysmography (cbPPG) is a non-contact measurement method, using video cameras and ambient light, which provides spatially resolved information about tissue perfusion. It has not been researched yet whether the measurement depth of cbPPG, which is limited by the penetration depth of ambient light, is sufficient to reach pulsatile vessels and thus to measure the perfusion strength in regions that are relevant for skin flap transplants. **Approach.** We applied constant negative pressure (compared to ambient pressure) to the anterior thighs of 40 healthy subjects. Seven measurements (two before and five up to 90 min after the intervention) were acquired using an RGB video camera and photospectrometry simultaneously. We investigated the performance of different algorithmic approaches for perfusion strength assessment, including the signal-to-noise ratio (SNR), its logarithmic components $\log S$ and $\log N$, amplitude maps, and the amplitude height of alternating and direct signal components. **Main results.** We found strong correlations of up to $r = 0.694$ ($p < 0.001$) between photospectrometric measurements and all cbPPG parameters except SNR when using the green color channel. The transfer of cbPPG signals to POS, CHROM, and O3C did not lead to systematic improvements. However, for direct signal components, the transformation to O3C led to correlations of up to $r = 0.744$ ($p < 0.001$) with photospectrometric measurements. **Significance.** Our results indicate that a camera-based perfusion strength assessment in tissue with deep-seated pulsatile vessels is possible.

1. Introduction

Despite careful execution, perfusion disorders of partial or complete skin flaps can occur after skin flap transplants due to arterial and venous stenosis, anastomoses, or the compression of pedicles due to swelling, twisting, or kinking. Perfusion disorders lead to insufficient oxygen supply and thus to necrosis of the skin flaps (Francis and Baynosa 2017). Postoperative perfusion strength monitoring can help to detect insufficient perfusion at an early stage and thus ensure the survival of the flap (Rahmanian-Schwarz *et al* 2012).

Physical examination, including visual color assessment or turgor, is still the clinical standard for skin flap monitoring (Patel *et al* 2017). Other methods, like laser Doppler flowmetry, photospectrometry, pulse oximetry, photoplethysmography (PPG), or tomographic approaches (Patel *et al* 2017, Kohlert *et al* 2019, Kyriacou *et al* 2020) are either invasive, expensive, complex, stationary, or contact-based. In case of post-surgery skin flap or wound monitoring, contact-based sensors must be applied to sensitive areas. However, there are several experimental studies on the non-contact flap viability assessment based on laser speckle (Carvalho Brinca *et al* 2021) or thermal

imaging (Hummelink *et al* 2020), near-infrared spectroscopy (Hill *et al* 2020), or camera-based photoplethysmography (Secerbegovic *et al* 2019). Camera-based photoplethysmography (cbPPG), also referred to as remote or imaging photoplethysmography or photoplethysmography imaging, is an optical measurement method that allows non-contact and continuous recording of cardio-respiratory signals and spatial information about tissue perfusion (e.g. perfusion strength) using video cameras and ambient light (Wu *et al* 2000, Huelsbusch and Blazek 2002, Verkruyse *et al* 2008). Due to the low penetration depth of ambient light, the exact origin of cbPPG signals is not completely understood (Verkruyse *et al* 2017). However, it is widely accepted that signal fluctuations can be attributed primarily to cutaneous blood volume fluctuations (Huelsbusch and Blazek 2002, Zauneder *et al* 2018). Therefore, cbPPG provides temporally and spatially resolved information about the perfusion strength.

The structure and diameter of the different skin layers and thus the depth of the blood vessels can vary considerably depending on the body region and individual (Kanitakis 2002). Therefore, feasibility studies for the cbPPG-based assessment of the perfusion strength on clinically relevant skin areas are needed. For skin flap transplants, the anterior thigh is of particular importance (Sun *et al* 2017). Two skin flaps (i.e. anterolateral and anteromedial) can be removed from the anterior thigh. Their size, skin quality, and vascular as well as nervous structure make them particularly suitable for large-area reconstructions with irregular shape (Song *et al* 1984).

With this paper we address the research gap in the field of cbPPG regarding non-contact perfusion strength assessment in the clinical setting of skin flap transplantation. For this purpose, we investigated the performance of various algorithmic approaches for perfusion strength assessment on camera recordings of the anterior thigh. In a clinical setup, continuous topical negative pressure wound therapy was used to influence regional cutaneous perfusion and photospectrometry at two different depths provided clinical reference measurements.

Even though cbPPG offers great potential, the technology is facing fundamental challenges that partly result from its vulnerability to motion artifacts (Zauneder *et al* 2018) and illumination fluctuations (Holton *et al* 2013) as well as the low penetration depth of ambient light (Verkruyse *et al* 2017). So far, most of the cbPPG-related research focuses on reliable heart rate (HR) and heart rate variability (HRV) measurement. Only few studies target the extraction of other parameters like perfusion strength or tissue oxygenation (Zauneder *et al* 2018). In section 2 we, therefore, sum up the research that has been conducted on perfusion strength assessment from cbPPG before we discuss the dependence of signal quality on the measurement region as well as color channel combinations for the mitigation of motion artifacts and lighting fluctuations. Section 3 introduces the methods used for signal processing and statistical evaluation. The results are presented in section 4 and discussed in section 5. Section 6 closes the paper with a conclusion and outlook.

2. Related work

2.1. Research on camera-based perfusion strength assessment

As mentioned before, it is assumed that (in line with conventional PPG) the cbPPG signal primarily results from blood volume effects in the measured area. Light that reaches the tissue is scattered, absorbed or reflected. A varying blood volume modulates the light that interacts with the tissue, which can be measured with photoelectric sensors (Hertzman 1937, Allen 2007). Hence, PPG as well as cbPPG signals correlate inverse to the blood volume, or more precisely to the amount of hemoglobin (Hb) in the measurement volume. The cbPPG signal can be divided into an alternating component (AC) and a direct component (DC). The AC reflects the blood volume fluctuations of the pulse wave triggered by the cyclic contraction of the heart (Reisner *et al* 2008). Permanent blood volume and low-frequency fluctuations resulting from respiration, vasomotor activity, blood pressure control mechanisms (Traube-Hering-Mayer waves), and thermoregulation are usually assigned to the DC (Nitzan *et al* 1994, Babchenko *et al* 2001, Reisner *et al* 2008). Therefore, Bousefsaf *et al* (2016) and Trumpp *et al* (2016) calculated the amplitude height from AC of spatially averaged signals as a correlate to arterial perfusion strength.

An amplitude map shows the spatially resolved local perfusion strength, realized by a pixel-wise calculation of perfusion strength parameters (Kamshilin *et al* 2011). The spatial representation enables regional differences to be assessed, but decreases processing speed and signal quality, which in turn can be improved by (grid-based) spatial averaging (Verkruyse *et al* 2008). Therefore, Verkruyse *et al* (2008) spatially averaged within a grid of 50×40 pixels before calculating the perfusion strength for each rectangle, i.e. the respective intensity at a reference HR. Yang *et al* (2015) applied filters on single pixel traces to diminish all frequencies deviating from a reference HR and calculated the perfusion strength of every pixel from the amplitude spectrum.

The approach of Kamshilin *et al* (2011) is based on the principle of synchronous demodulation by multiplying the pixel time series with a carrier function. The carrier function is derived from the estimated HR and its first harmonic (± 5 beats per minute (bpm)) of the spatially averaged pixel values. The complex carrier function is normalized to 1 and then multiplied by the pixel values, which corresponds to a lock-in amplification

of HR-synchronous pixel value fluctuations. The resulting pixel values are summed up over time. The magnitude of the resulting complex correlation matrix corresponds to the amplitude map (Kamshilin *et al* 2011).

Zaunseder *et al* (2018) use the approach from Kamshilin *et al* (2011) but form the carrier function from a single frequency equal to the HR. As a result, the amplitudes are constant but no HRV is considered, which leads to less physiologically inexplicable fluctuations (Fleischhauer *et al* 2019).

All previous approaches only consider the HR-synchronous AC, which primarily relates to the arterial vascular system. Marcinkevics *et al* (2016) and Rasche *et al* (2020) introduced a perfusion index PI as the ratio of the AC to the DC. Secerbegovic *et al* (2019) and Zaunseder *et al* (2018) used the signal-to-noise ratio (SNR) according to de Haan and Jeanne (2013), which originally is a measure for signal quality, to estimate the perfusion strength. The SNR is calculated from the ratio of the HR synchronous energy (Signal) to the of the signal's energy (Noise) and thus increases with an increasing ratio of AC to DC (de Haan and Jeanne 2013). Both parameters, PI and SNR, can be understood as a ratio of the HR-synchronous AC to the low-frequency DC. Therefore, simultaneous effects in high and low frequency blood volume fluctuations can compensate each other.

He and Wang (2020) calculated the amount of oxy- and deoxygenated Hb in the entire arteriovenous plexus from the intensities of three closely adjacent wavelength bands with the associated extinction coefficients of oxy- and deoxygenated Hb. They used a Wiener matrix to reconstruct hyperspectral images from RGB images. Since the extinction coefficients are wavelength-dependent, the illumination's spectral power distribution strongly influences the approach (He and Wang 2020), which requires thorough calibration and constant illumination.

2.2. Measurement location dependency in camera-based photoplethysmography

Research papers from the field of cbPPG mostly focus on easily accessible and well-perfused measurement areas like the face, which increases the signal quality and thus the accuracy of HR measurement (Zaunseder *et al* 2018).

The skin consists of three main layers: the outermost and bloodless epidermis, the dermis, and the subcutis (Kanitakis 2002). With regard to the enclosed vessels, the dermis can be subdivided (with increasing depth) into the papillary dermis, the superficial arteriovenous plexus, the reticular dermis, and the deep arteriovenous plexus (Bashkatov *et al* 2005). While the papillary dermis is interwoven with non-pulsatile capillaries, the other three layers also contain arterioles beside venules and thus pulsatile vessels (Bashkatov *et al* 2005).

Depending on the penetration depth⁵ of the ambient light into the skin, which is approximately 1.8 mm for light from red wavelengths and less for lower wavelengths (Trumpp 2019), and the thickness of the epidermis, which can vary significantly regionally and individually (Kanitakis 2002), ambient light reaches tissue which contains pulsatile vessels, i.e. minimum upper vascular plexus.

Measurements by Kakasheva-Mazhenkovska *et al* (2011) indicate that the pulsatile vessels at the anterior thigh are situated deeper than at the forehead because of a thicker papillary dermis⁶, even if the epidermis at the thigh is thinner than at the forehead⁷. To the best of our knowledge, there are no works applying cbPPG to assess the perfusion strength on the anterior thigh, even though this is of great importance to skin flap transplantation.

2.3. Research on color channel combinations

Most cbPPG setups use RGB cameras that provide an (R), a (G), and a (B) color channel for each pixel (Zaunseder *et al* 2018). The color channels contain different information (e.g. information from different tissue depths (Mishra *et al* 2017) and absorption bands (Addison *et al* 2017)). Due to the strong absorption of green light by Hb, the G channel provides the best SNR and is therefore favored (Verkruyse *et al* 2017). However, comparative studies (Tsouri and Li 2015, Ernst *et al* 2020, 2021) have shown that separation of color information, e.g. into hue, saturation, and luminance, through transformation into other color spaces can significantly improve the accuracy of HR measurement. This is due to lower susceptibility to unsteady illumination or small movement artifacts of some of these color spaces' channels (Tsouri and Li 2015).

In darker skin types fewer photons contribute to the pulsatile signal due to an increased constant photon absorption by an elevated melanin concentration in the epidermis. This reduces the signal intensity and thus also the signal quality but not the spectral absorption characteristics of Hb (de Haan and Jeanne 2013). CHROM (de Haan and Jeanne 2013) and POS (Wang *et al* 2017) assume a standardized skin tone

$$[R_s, G_s, B_s] = [R, G, B] / \sqrt{R^2 + G^2 + B^2} = [0.7682, 0.5121, 0.3841] \quad (1)$$

that is similar for every skin tone under white light as described by de Haan and Jeanne (2013). CHROM uses two orthogonal chrominance signals to eliminate specular reflections, and skin color standardization as well as

⁵ Defined as the depth, at which the light has still 37% of its incident intensity.

⁶ Average thickness of 107.9 μm at the forehead and 314.9 μm at the anterior thigh for people between the ages of 23 and 53 years.

⁷ Average thickness of 244.4 μm at the forehead and 143.9 μm at the anterior thigh for people between the ages of 23 and 53 years.

Table 1. Algorithmic implementation of CHROM (de Haan and Jeanne 2013) and POS (Wang *et al* 2017). RGB color channels are temporally normalized, expressed with subscript n in both cases, and included in the calculation of the chrominance signals X and Y . α is recalculated as the ratio of the chrominance signals' standard deviations σ for every window, whereas the subscript f indicates an upstream band-pass filter for CHROM. Calculations are carried out for overlapping windows of 1.6 s and combined to form a signal S by means of Hanning windows (CHROM) or overlap adding (POS).

Variable	CHROM	POS
X	$3R_n - 2G_n$	$G_n - B_n$
Y	$1.5R_n + G_n - 1.5B_n$	$-2R_n + G_n + B_n$
α	$\sigma(X_f)/\sigma(Y_f)$	$\sigma(X)/\sigma(Y)$
$S(\alpha)$	$X_f - \alpha Y_f$	$X + \alpha Y$

α -amplitude tuning to correct violations of white illumination (de Haan and Jeanne 2013). POS follows the same approach but with a projection orthogonal to the skin color (Wang *et al* 2017). The main components of the algorithmic implementation of CHROM and POS can be found in table 1. Due to the α -amplitude tuning, both approaches are time dynamic, which leads to an elimination of DC and can alter cbPPG signal morphology (Ernst *et al* 2021). Therefore, Ernst *et al* (2021) empirically derived an optimal linear RGB color channel combination (O3C)

$$S_{O3C} = 0.25R - 0.83G + 0.5B \quad (2)$$

for skin tone independent HR measurement that outperformed conventional color channels and preserves the DC.

3. Material and methods

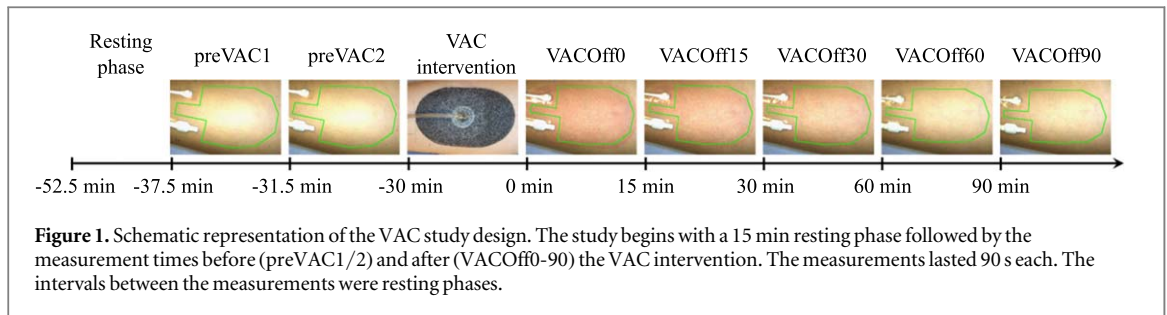
3.1. Data material and study design

In contrast to most cbPPG studies, our study focuses on the anterior thigh to assess changes in perfusion strength in a clinical setting. Our study design is based on previous work by Muenchow *et al* (2019) in which continuous topical negative pressure wound therapy was used to increase regional tissue perfusion in healthy subjects beyond the duration of the intervention. Our study was approved by the Institutional Review Board of TU Dresden (EK495122018) in accordance with the Helsinki Declaration.

Measurements on 40 healthy subjects (male: 20) with an average age of 27.0 ± 4.1 years were recorded with an RGB camera (UI-3060CP-C-HQ Rev. 2, IDS Imaging Development Systems GmbH, Obersulm, Germany, 100 frames per second (fps), 604×608 pixels, RGB 3 \times 12 bit) at a distance of approximately 60–100 cm. A lens (Cinegon 1.8/16 0901, Jos. Schneider Optische Werke GmbH, Bad Kreuznach, Germany) with 16 mm focal length was mounted on the camera. To enable individual illumination adaption for each subject, a dimmable cold light source in form of a light emitting diode (LED) ring (MIC-209; EPE (HengYang) Apparatus Light Factory, Hengyang, China) was attached around the camera.

Reference measurements were recorded with the oxygen to see[®] (O2C[®]) device from LEA Medizintechnik GmbH (Gießen, Germany). By combining white light spectroscopy (450–1000 nm) and laser Doppler flowmetry (820 nm), the O2C[®] device measured the regional Hb concentration (rHb), the oxygen saturation (sO₂), the blood flow (Flow), and the blood flow velocity (Velocity). Flow and rHb are directly related to temporal fluctuations of the regional amount of Hb and are therefore suitable as reference parameters for cbPPG. The use of two different sensors, each with different distances between photo sensor and light source, allows to measure at two different depths, i.e. 3 and 7 mm. The O2C[®] parameters refer to the arteriovenous system. Since the proportion of venous blood clearly predominates in the vascular system (i.e. 75% of total blood volume), the measured values are dominated by venous components (Krug 2006).

For stimulating the tissue perfusion on the anterior thigh, we used the vacuum-assisted-closure (VAC) system ACTIV.A.C.[™] by KCI Medizinprodukte GmbH (Wiesbaden, Germany) and created a constant negative pressure (compared to ambient pressure) of 125 mmHg for 30 min. Figure 1 shows the design of the VAC study. Prior to the first measurement, the subjects spent a 15 min resting phase (already in the measuring position), firstly to minimize influences from previous physical stress and secondly to avoid technical interference from heating processes of the camera. The resting phase was followed by two measurements (preVAC1 and preVAC2), the 30 min VAC intervention and another five measurements 0, 15, 30, 60, and 90 min after the intervention (VACOff0 to VACOff90). At each of these seven measurement times, video recordings with a



length of 90 s and O2C[®] measurements were carried out simultaneously. The subjects remained in a lying position the entire time. They were instructed not to speak during the measurements and to move as little as possible. The pilosity was removed beforehand.

3.2. Signal extraction and color channel combination

For signal extraction, the region of interest (ROI) was defined manually for each 90 s video enclosing the whole area of the VAC sponge (ROI1). In some videos (especially during preVAC1 and preVAC2) spots of saturated pixels on the top of the thighs (see figure 2) were observed, which indicates that blood volume fluctuations cannot be mapped correctly by the corresponding pixel values. Therefore, a second ROI (ROI2) was generated. ROI2 contained only those pixels of ROI1 in which neither of the color channels reached saturation during a measurement.

Channel-wise spatial averaging of pixel values within each ROI was performed to reduce noise and thus to improve the signal quality (Verkrusse *et al* 2008). For spatially resolved approaches (i.e. amplitude maps), the pixel values were retained.

CHROM, POS and O3C (in the following simply referred to as color channels) were applied to the spatially averaged and spatially resolved RGB signals. For CHROM and POS we used the *iPhys toolbox* (McDuff 2020) for Matlab. O3C was implemented according to equation (2) (Ernst *et al* 2021). Pixel-wise transformation was only carried out for ROI2, since the missing pixel fluctuations in saturated pixels of ROI1 distort the α amplitude tuning of POS and CHROM as well as the channel combination of O3C. The superimposition of 1.6 s windows in POS and CHROM required the omission of the first and last 0.8 s of each measurement. Therefore, we used 8 consecutive 10 s windows (no overlap) to calculate the perfusion strength parameters. With 40 subjects and 7 measurement times, our study provided a total sample size of 2240 10 s windows. Figure 2 summarizes the approaches of signal processing and the calculation of perfusion strength parameters. All signal processing was executed in Matlab R2020b (MathWorks, Inc., Natick, Massachusetts, USA).

3.3. Perfusion strength parameter calculation

The O2C[®] parameters relate to arteriovenous vasculature. Measurements from Enezi *et al* (2015) on 103 subjects of different age groups (21 of them with cardiovascular diseases) show a strong correlation between arterial and venous amount of Hb ($r = 0.774, p < 0.01$). Therefore, cbPPG parameters based on the AC (mainly arterial effects) were calculated as well as parameters based on the DC (low-frequency arteriovenous effects).

3.3.1. Amplitude height

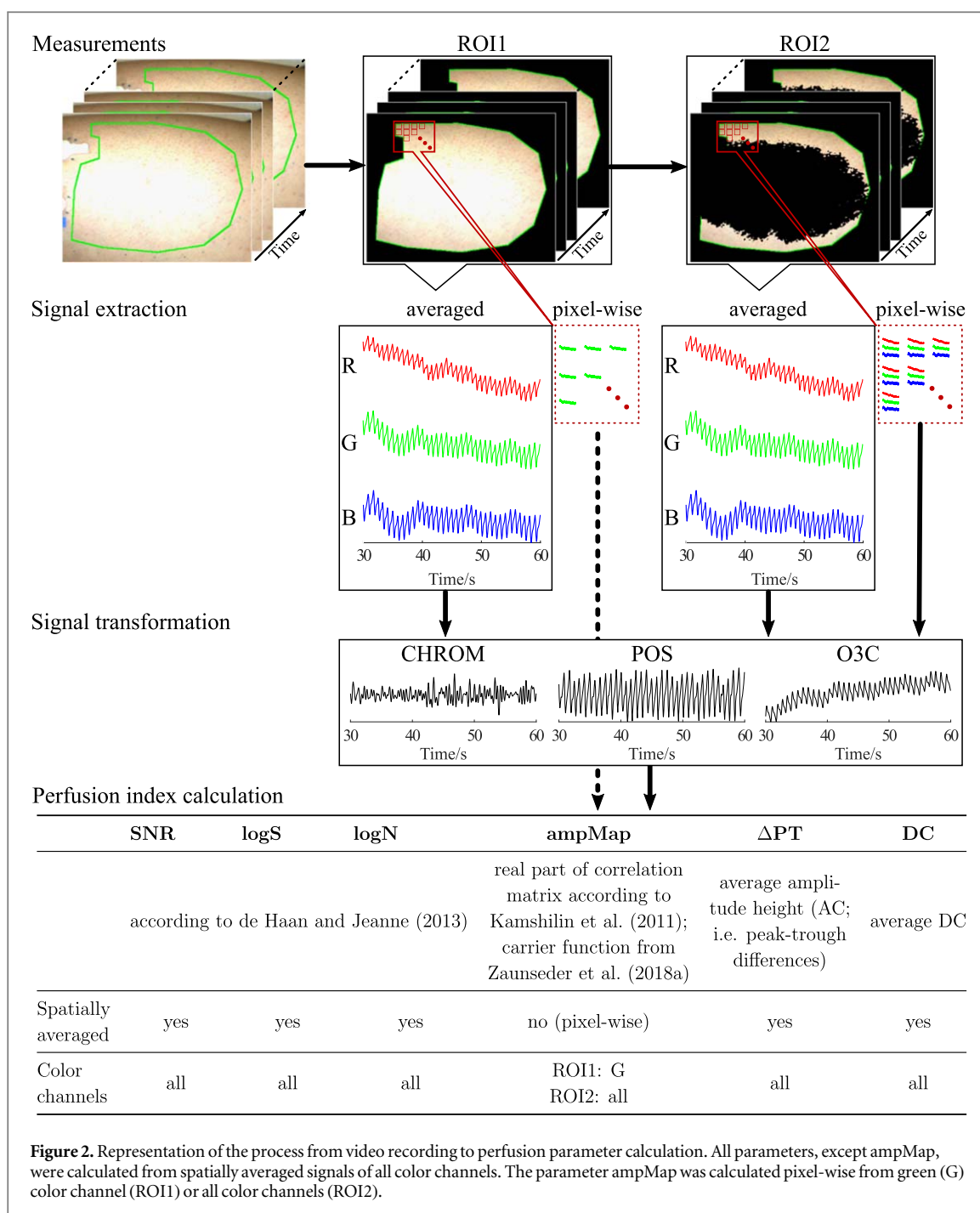
AC and DC were extracted from the spatially averaged signals of all color channels (G, CHROM, POS and O3C) by using a band pass (AC) or low-pass (DC) filter. We used 5th order Butterworth filters with cut-off frequencies at 0.5 and 3.3 Hz for AC and 0.5 Hz for DC. Amplitude height was calculated from AC as the peak-trough difference (ΔPT). For identifying peaks and troughs, we used the Matlab function `findpeaks()` with a minimum peak-to-peak distance of 0.3 s, a minimum prominence ($0.5 \cdot \text{mean}(|AC|)$) and a minimum height ($\max[0.1 \cdot \text{median}(|AC|), 0]$). The parameter DC was calculated as the arithmetic mean of the DC over the entire window length.

3.3.2. Amplitude maps

Amplitude maps as a measure of the perfusion strength were calculated according to Kamshilin *et al* (2011). However, we followed a more recent approach described by Zaunseder *et al* (2018) to generate the reference function based on a single frequency (corresponding to the HR).

Each of the spatially resolved time series (G for ROI1; G, CHROM, POS and O3C for ROI2) were detrended with the Matlab function `detrend()` and band-pass filtered between 0.5 and 6 Hz (5th order Butterworth).

For each color channel, a sine function oscillating with the estimated HR was used as carrier function respectively. To compute the estimated HR, the signals were spatially averaged within the respective ROI and



transferred to the frequency domain using fast Fourier transformation (FFT). The HR was defined as the frequency with the maximum energy between 0.5 and 3.3 Hz, which corresponds to a HR between 30 and 200 bpm. In line with Zaunseder *et al* (2018), the spectral power of all other frequencies was set to zero. The carrier functions were generated with the inverse FFT of the manipulated spectra and normalized to the value range between -1 and 1.

The spatially resolved signals were multiplied with the carrier function, which led to complex time series. Integration over time yielded a spatially resolved complex correlation matrix. Contrary to Kamshilin *et al* (2011), we used the real part of this matrix which contains fluctuations that are in phase with the carrier function to form the amplitude map. By spatially averaging the amplitude map we derived the perfusion strength index *ampMap*.

3.3.3. Signal-to-noise ratio

After linear detrending, the spatially averaged signals (both ROIs and all color channels) were band-pass filtered (5th order Butterworth) between 0.5 and 6 Hz and transferred to the frequency domain using FFT. Then, SNR was calculated according to de Haan and Jeanne (2013) as the sum of all amplitude values X of those frequencies f

included within the ± 5 bpm frequency bands around the HR frequency f_{hr} or its first harmonic f_{hr1} in relation to the remaining amplitude spectrum:

$$SNR = 10 \log_{10} \left(\frac{\sum_{f=\lambda_1}^{\lambda_2} \Pi(f) |X(f)|^2}{\sum_{f=\lambda_1}^{\lambda_2} (1 - \Pi(f)) |X(f)|^2} \right). \quad (3)$$

By using the binary mask

$$\Pi(f) = \begin{cases} 1, & \text{if } |f_{hr} - f| \leq 5 \text{ bpm} \\ 1, & \text{if } |f_{hr1} - f| \leq 5 \text{ bpm}, \\ 0, & \text{else} \end{cases} \quad (4)$$

the frequency range was limited to $\lambda_1 \leq f \leq \lambda_2$ with $\lambda_1 = 30$ bpm and $\lambda_2 = 200$ bpm. As described before, f_{hr} corresponds to the frequency with the maximum energy in the spectral power distribution.

In addition to the SNR, we considered signal and noise (numerator and denominator in equation (3)) individually. Both, signal and noise, were scaled using the decadic logarithm, and we refer to them as logS and logN respectively.

3.4. Statistics

3.4.1. General linear mixed model

Due to the complex setting with various possible influencing factors (including ROI and color channel), multiple GLMMs—one for every cbPPG parameter—were performed to examine which factors influence the cbPPG parameters significantly (section 3.4.1). Based on this, we performed linear relationship analysis between cbPPG and O2C® parameters to validate the used algorithms (section 3.4.2). All statistics were done with IBM® SPSS® Statistics 27 (IBM Corporation; Armonk (NY), USA).

GLMMs belong to the linear regression models and allow to analyze the influence of multiple factors on an outcome variable, that does not have to be normal distributed (Williams 1982, Breslow 1984) and may underlay additional random effects (Breslow and Clayton 1993) in a repeated measures design (Clayton and Kaldor 1987).

We carried out one GLMM analysis per cbPPG parameter, with the respective cbPPG parameter defined as target variable. Repeated measures were defined as a coupling between measurement time and signal-processing window with diagonal covariance. Gender, age, body-mass index (BMI), color, ROI and measurement time were defined as fixed factors, and subjects were defined as random factors. The maximum number of iterations was set to 100, the confidence level to 95%, and due to the large sample size, the residual method was chosen for the calculation of degrees of freedom.

3.4.2. Correlation analysis

Linear relationship analyses were performed between O2C® and cbPPG parameters, in consideration of the factors that have significant influence (identified by the GLMMs). For eliminating inter-individual base-level differences, all parameter values (cbPPG and O2C®) were normalized to a baseline by subtraction. The baseline was calculated for each parameter as the subject-dependent average of the parameter values, derived from eight consecutive windows, at preVAC2.

Two bivariate normally distributed parameters with at least interval-scaled data can be tested for linear relationship using the *Bravais-Pearson* correlation coefficient r (Bortz and Schuster 2010). Therefore, all parameters were checked for normal distribution using the *Kolmogorov-Smirnov* and *Shapiro-Wilk* tests. In case of no normal distribution is found, the calculation of *Spearman's* rank correlation coefficient ρ as a measure for monotone relationship is indexed (Bortz and Schuster 2010). However, in compliance with the central limit theorem, the superposition of independent random effects leads to an approximately normal distribution in large samples (Bortz and Schuster 2010), which can be assumed in our study with 2240 values for each parameter. Therefore, *Bravais-Pearson's* correlation coefficient r was used.

4. Results

4.1. Significant influencing factors

The results of GLMM in table 2 indicate a significant influence of the factors color channel and measurement time on all cbPPG parameters. Furthermore, all parameters except logN ($p = 0.189$) are influenced by the choice of ROI. Gender, age, and BMI were no significant influencing factors. Therefore, in correlation analysis, we considered all parameters separately for different color channels and ROIs.

Since the GLMM showed that the ROI was not a significant factor for all cbPPG parameters, we tested for consistency between both ROIs by examining a two-way mixed intraclass correlation (ICC) analysis (adjusted to

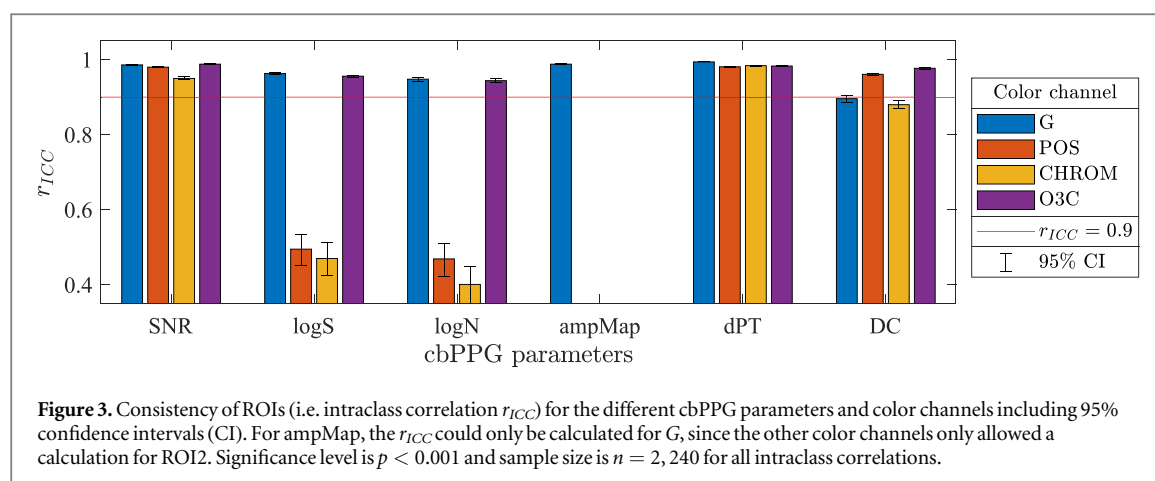


Table 2. Significance levels p , extracted from the results of the generalized linear mixed models (GLMMs), with fixed and random effects on cbPPG parameters.

	p -value SNR	p -value logS	p -value logN	p -value Δ PT	p -value DC	p -value ampMap
Fixed effects						
Corrected model	***	***	***	***	***	***
Gender	0.958	0.253	0.256	0.335	0.130	0.532
Age	0.939	0.475	0.439	0.468	0.276	0.780
BMI	0.808	0.773	0.692	0.828	0.507	0.794
Color	***	***	***	***	***	***
ROI	*	*	0.189	***	***	***
Time	***	***	***	***	***	***
Random effects						
	***	***	***	***	***	***

* $p < 0.05$; *** $p < 0.001$.

mean differences between ROIs). The value range of ICCs is between -1 and 1 , whereby an ICC of $r_{ICC} = 0$ means no consistency and $|r_{ICC}| = 1$ means 100% consistency (Koo and Li 2016). Our results of ICC analysis are shown in figure 3. A consequently excellent consistency between the values of both ROIs was found in case of O3C. For DC, the ICCs were just below the threshold for excellent consistency for G ($r_{ICC} = 0.896$) and for CHROM ($r_{ICC} = 0.870$). In case of G, the upper bound of the confidence interval with $r_{ICC} = 0.905$ was barely above the threshold. With ICCs ranging between $r_{ICC} = 0.401$ and $r_{ICC} = 0.495$, no excellent consistency between both ROIs could be found for logS and logN when using POS or CHROM.

4.2. Influence of the intervention on perfusion strength

As it can be seen in figure 4, the continuous topical negative pressure wound therapy effects rHb, Flow and sO_2 at both measurement depths in the form of a temporary increase (Flow deep and surface, rHb surface, and sO_2 surface) or decrease (rHb deep). The extent of the effect differs for surface and deep measurements as the median change from preVAC2 to VACOff0 was $+41.9$ a. u. for Flow, $+19.9$ a. u. for rHb, and $+30.2$ percentage points (p. p.) for sO_2 in the surface measurements and $+49.7$ a. u. for Flow, -3.9 a. u. for rHb, and $+1.7$ p. p. for sO_2 in the deep measurements. In the following 90 min, the values moved towards the level of preVAC2, but especially the values of the surface measurements remained slightly increased (Flow: $+6.4$ a. u., rHb: $+6.8$ a. u., and sO_2 : $+4.1$ p. p.). Bota et al (2022) have examined the effect more closely based on the same data.

4.3. Relationship between reference and camera-based perfusion strength assessment

According to Shapiro–Wilk test, none of the parameters met the normal distribution requirement (see appendix A, table A1). Table 3 shows the results of the correlation analysis. Correlations are highlighted by color referring their strength according to Cohen (1988): $|r| \geq 0.1$ implies a weak, $|r| \geq 0.3$ a moderate, and $|r| \geq 0.5$ a strong linear relationship between two variables. In case of an excellent consistency between both ROIs, we only included the ROI with stronger correlations in table 3. A full correlation table including Spearman's ρ , both ROIs and all O2C® parameters is attached in appendix B (table B1).

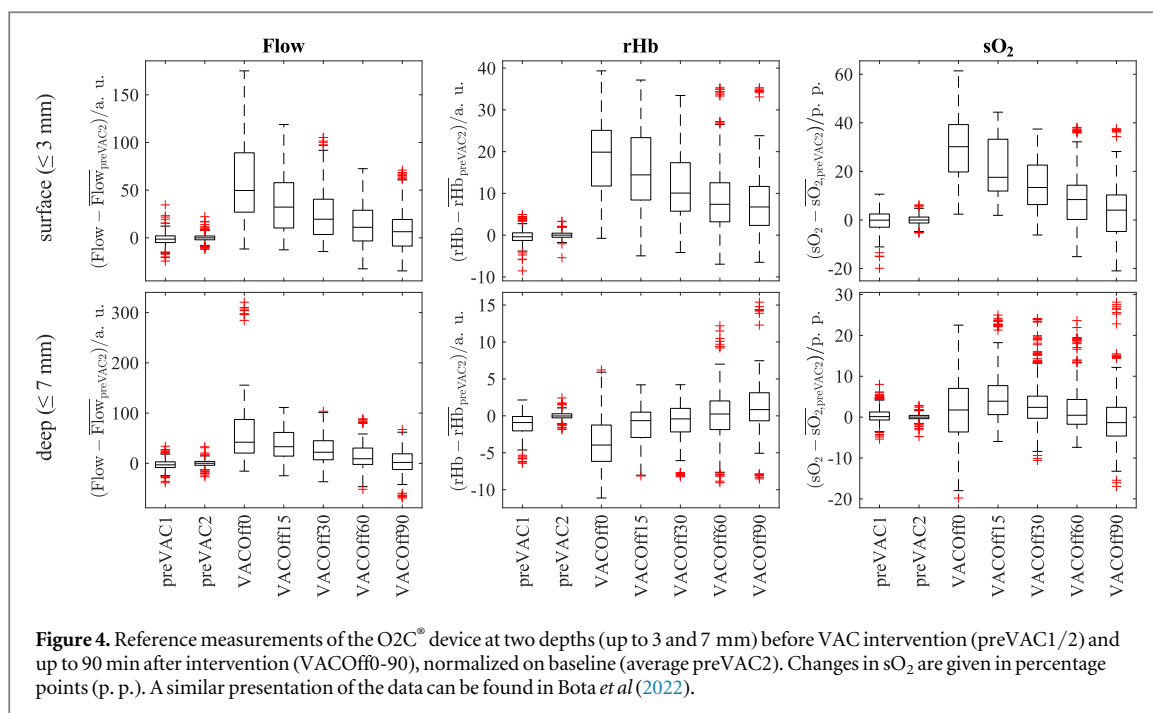


Figure 4. Reference measurements of the O2C[®] device at two depths (up to 3 and 7 mm) before VAC intervention (preVAC1/2) and up to 90 min after intervention (VACOff0-90), normalized on baseline (average preVAC2). Changes in sO₂ are given in percentage points (p. p.). A similar presentation of the data can be found in Bota *et al* (2022).

Strong correlations were found between all cbPPG parameters (except SNR) and the O2C[®] parameters Flow (deep and surface) and rHb (surface). In addition, we found strong correlations between almost all cbPPG parameters and the sO₂ (surface).

In case of some cbPPG parameters (in particular logS, logN and, DC), the choice of color channel has a strong influence on the correlations to the reference parameters. G and O3C perform significantly better for all of these three cbPPG parameters and slightly better for Δ PT (across all O2C[®] parameters), whereby for DC O3C outperforms G. Only in the case of ampMap the correlations of all color channels are on a comparable level.

5. Discussion

The O2C[®] measurements relate to the arteriovenous vascular system and are approximated as venous parameters due to the dominance of venous blood volume (Krug 2006). Classically, cbPPG parameters are calculated from AC and thus refer primarily to pulsatile Hb fluctuations in the arterial vascular system (Huelsbusch and Blazek 2002). Nevertheless, concerning the correlation between the arterial and the venous amount of Hb (Enezi *et al* 2015), we implemented some classical approaches (i.e. SNR, logS, logN, Δ PT, and ampMap). DC includes low-frequency signal fluctuations and hence, like O2C[®] parameters, relates to the arteriovenous vascular system. Regardless of the cbPPG signal origin, we found equally strong correlations between cbPPG parameters and O2C[®] parameters rHb and Flow. There are (a) physiological or (b) device-related explanatory approaches for this:

- Since the effect of continuous topical negative pressure wound therapy (performed here using the VAC device) on local perfusion is not yet fully understood (Muenchow *et al* 2019), it is conceivable that arterial and venous blood volumes are increased equally. The two vascular systems form a closed system. If blood accumulates in a part of the venous vascular system, there is either a venous stenosis/occlusion or a regionally increased arterial inflow due to dilatation of the upstream arterial vessels (Brandes and Busse 2011). The latter affects cbPPG parameters with arterial reference as shown by Trumpp *et al* (2016).
- Although venous effects are overrepresented in O2C[®] measurements, they also contain arterial effects (Krug 2006). Thus, strong arterial effects, which may be provoked by VAC intervention, appear in both cbPPG and O2C[®] measurements.

The measurement depth of cbPPG is determined by the penetration depth of visible light, which is approximately 1.8 mm for red light and less for lower wavelengths (Bashkatov *et al* 2005). Keeping the tissue characteristics in mind (section 2.2), it is plausible that we found strong correlations between cbPPG and more superficial O2C[®] parameters. In contrast, strong correlations of almost all cbPPG parameters with Flow, measured in up to 7 mm, were less to be expected. Since the O2C[®] parameters are calculated based on sum

Table 3. Bravais-Pearson's correlation coefficients r between reference O2C[®] parameters and cbPPG parameters for different color channel combinations and ROIs. Correlation strengths according to Cohen (1988) are highlighted by color and significance levels by stars (see legend). If consistency between ROIs was found in intraclass correlation analysis (see figure 3), the ROI with the stronger correlations is shown.

cbPPG parameter	color channel	ROI	O2C [®] parameter					
			Flow		rHb		sO ₂	
			deep	surface	deep	surface	deep	surface
SNR	G	2	0.133***	0.070**	-0.100***	0.032	-0.050*	0.121***
	POS	1	0.123***	0.061**	-0.027	0.012	-0.063	0.060**
	CHROM	2	0.090***	0.013	-0.033	0.014	-0.072**	0.070**
	O3C	2	0.122***	0.038	-0.062**	-0.003	-0.046*	0.080***
logS	G	1	0.580***	0.616***	-0.358***	0.617***	0.144***	0.617***
	POS	1	-0.045*	-0.047*	-0.102***	-0.011	0.073**	-0.017
		2	-0.045*	0.014	-0.064**	0.013	0.112***	0.051*
	CHROM	1	-0.097***	-0.099***	0.105***	-0.088***	0.049*	-0.054*
		2	-0.070**	0.048*	-0.125***	-0.011	-0.042*	-0.036
	O3C	1	0.606***	0.680***	-0.364***	0.673***	0.209***	0.643***
logN	G	1	0.521***	0.571***	-0.298***	0.527***	0.096***	0.515***
	POS	1	-0.008	-0.018	-0.107***	0.017	0.081***	0.024
		2	-0.016	0.025	-0.060**	0.014	0.124***	0.630**
	CHROM	1	-0.062**	-0.086***	0.120***	-0.109***	0.035	-0.068**
		2	-0.037**	0.068**	-0.114***	0.004	-0.064**	-0.041
	O3C	1	0.584***	0.665***	-0.323***	0.623***	0.189***	0.594***
ampMap	G	1	0.673***	0.669***	-0.426***	0.658***	0.162***	0.746***
	POS	2	0.651***	0.664***	-0.403***	0.606***	0.112***	0.709***
	CHROM	2	0.624***	0.646***	-0.401***	0.599***	0.114***	0.727***
	O3C	2	0.612***	0.611***	-0.412***	0.575***	0.096***	0.735***
ΔPT	G	2	0.698***	0.694***	-0.418***	0.664***	0.181***	0.748***
	POS	1	0.580***	0.550***	-0.338***	0.614***	0.162***	0.735***
	CHROM	2	0.656***	0.660***	-0.394***	0.631***	0.156***	0.736***
	O3C	1	0.685***	0.640***	-0.415***	0.651***	0.163***	0.755***
DC	G	1	-0.610***	-0.659***	0.219***	-0.678***	-0.194***	-0.585***
		2	-0.566***	-0.614***	0.241***	-0.573***	-0.237***	-0.603***
	POS	2	-0.055*	-0.041	0.039	-0.038	-0.006	-0.064**
	CHROM	1	0.031	0.055**	-0.019	0.031	0.008	0.037
		2	0.090***	0.091***	-0.014	0.065**	-0.005	0.055**
	O3C	2	0.670***	0.736***	-0.270***	0.744***	0.332***	0.717***

● $|r| \geq 0.1$; ● $|r| \geq 0.3$; ● $|r| \geq 0.5$
 * $p < 0.05$; ** $p < 0.01$; *** $p < 0.001$
 $n = 2, 240$

signals, a possible explanation is that the change in Flow results primarily from superficial effects that are recorded by both measuring probes. Another explanation is that the Flow is equally influenced in different depths.

Also, as sO₂ is not directly connected to perfusion strength it was not expected that the cbPPG parameters (especially ΔPT) correlated strongest with surface sO₂. The reason for this could be a combination of three factors: first, stronger arterial perfusion, which can be measured with the cbPPG parameters ΔPT, ampMap, and logS, leads to an increased arteriovenous sO₂ if venous blood volume keeps constant. Second, it can be assumed that if arterial sO₂ and the oxygen consumption in the cells remain the same, the venous sO₂ is also increased due to an increased supply of oxygen that comes along with stronger arterial perfusion. Third, the absorption characteristics of Hb change depending on the sO₂, which, depending on the color channel, might increase the signal quality and intensity.

The strong correlations of logS and logN for color channels G and O3C with different O2C[®] parameters indicate a change in the frequency-dependent signal energy, both around the HR and its first harmonic (logS) and in the remaining frequency range (logN) as a result of altered arteriovenous sO₂, perfusion strength and/or blood volume. When calculating SNR, the effects on logS and logN seem to balance each other out, so that the VAC effect is hardly reflected in SNR.

In contrast to POS and CHROM, O3C retains the DC and thus, also when used in combination with logS, logN, and DC, O3C achieves strong correlations with O2C[®] parameters. In general, competitive results are achieved with the relatively simple color channels G and O3C, although O3C is not adapted to the examined data

set (i.e. illumination, skin tones). A conversion to POS and CHROM is therefore not worthwhile for perfusion strength assessment.

In summary, our results indicate that the penetration depth of light into the tissue is sufficient to even reach deep-seated pulsatile vessels such as those on the anterior thigh. Thus, perfusion strength assessment with cbPPG seems to be conceivable in clinical applications like skin flap transplantation or others such as wound healing assessment or the monitoring of ischemic extremities. However, our attempts to explain the relationships between different cbPPG and O2C[®] parameters are based on the assumption of healthy subjects. Therefore, it is questionable whether these relationships similarly exist in patients with cardiovascular diseases, metabolic disorders, or similar diseases. Furthermore, the applicability to flaps with inhibited perfusion is to be investigated. Automatic pre-measure adjustment of the LEDs' intensity could thereby help to prevent pixel saturation. However, it should be noted that the intensity must not change between measurements on the same subject.

The arithmetic averaging of the pixel values within ROIs is based on the assumption that the regional perfusion strength is changed in the whole region. However, ampMaps could also provide valuable information in the case of partial perfusion disorders in which only parts of the skin flap are insufficiently perfused and thus at risk from necrosis.

The explanatory power of statistical significance is restricted by the large size of the dataset and multiple testing without alpha correction. As the Bravais-Pearson correlation only considers linear relationships, we tested Spearman correlation with similar results.

6. Conclusion

The aim of our study was to investigate the feasibility of assessing changes in perfusion strength using cbPPG regarding a future clinical application, for which we evaluated ROIs on the anterior thigh as a relevant area for skin flap transplants. We exposed the tissue to negative pressure (compared to ambient pressure) for 30 min with the clinically established VAC system to influence the regional perfusion. The O2C[®] device, a clinically established device for assessing tissue metabolism, was used as a reference.

We applied various parameters for evaluating the perfusion from cbPPG signals to a data set consisting of 2,240 10 s segments from 40 subjects and found strong correlations with the perfusion-related O2C[®] parameters rHb and Flow. The transfer of cbPPG signals to POS, CHROM, and O3C did not lead to systematic improvements compared to the G channel. Parameters based on O3C (except ΔPT and ampMap) correlated slightly stronger with reference parameters compared to the G channel and, in contrast to POS and CHROM, O3C retained the DC.

Our study thus provides valuable information that a camera-based perfusion strength assessment in tissue with deep-seated pulsatile vessels is possible, which, in addition to postoperative skin flap monitoring, can be relevant for monitoring wound healing or ischemic extremities. Future research should focus on approaches for artifact suppression that maintain the DC, on validation of cbPPG parameters with the help of separate arterial and venous reference measurements, and on targeted influencing of individual perfusion parameters. Our results should also be verified in patients with cardiovascular disease or metabolic disorders and in skin flaps that are insufficiently perfused.

Acknowledgments

This work was partially supported by grants from the European Union's Horizon 2020 research and innovation programme (TIMELY, No 101 017 424) and the German Research Foundation (DFG, Deutsche Forschungsgemeinschaft) as part of Germany's Excellence Strategy (F-003661-553Ü4G-1250000, subproject 4G of 'The synergetic university').

Appendix A. Test for normal distribution

Table A1. Results from tests for normal distribution including the statistics for Kolmogorov–Smirnov and Shapiro–Wilk tests and the significance (p -value). Tests were applied to the cbPPG and the O2C[®] data. No subdivision according to measurement times and no sorting out of outliers was carried out.

		Kolmogorov–Smirnov				Shapiro–Wilk			
		Statistics		p		Statistics		p	
		Deep	Surface	Deep	Surface	Deep	Surface	Deep	Surface
O2C [®] parameter									
Flow		0.137	0.161	<0.001	<0.001	0.831	0.835	<0.001	<0.001
rHb		0.085	0.119	<0.001	<0.001	0.955	0.914	<0.001	<0.001
sO₂		0.139	0.109	<0.001	<0.001	0.898	0.952	<0.001	<0.001
Velocity		0.086	0.149	<0.001	<0.001	0.969	0.889	<0.001	<0.001
cbPPG parameter	Color channel	ROI1	ROI2	ROI1	ROI2	ROI1	ROI2	ROI1	ROI2
SNR	G	0.048	0.043	<0.001	<0.001	0.990	0.990	<0.001	<0.001
	POS	0.059	0.063	<0.001	<0.001	0.984	0.984	<0.001	<0.001
	CHROM	0.061	0.066	<0.001	<0.001	0.979	0.979	<0.001	<0.001
	O3C	0.069	0.068	<0.001	<0.001	0.981	0.980	<0.001	<0.001
logS	G	0.041	0.024	<0.001	0.006	0.989	0.991	<0.001	<0.001
	POS	0.137	0.110	<0.001	<0.001	0.949	0.957	<0.001	<0.001
	CHROM	0.052	0.103	<0.001	<0.001	0.993	0.968	<0.001	<0.001
logN	O3C	0.035	0.015	<0.001	0.200 ^a	0.990	0.995	<0.001	<0.001
	G	0.021	0.016	0.027	0.200 ^a	0.997	0.997	<0.001	<0.001
	POS	0.142	0.123	<0.001	<0.001	0.946	0.940	<0.001	<0.001
	CHROM	0.059	0.108	<0.001	<0.001	0.994	0.966	<0.001	<0.001
ampMap	O3C	0.015	0.021	0.200 ^a	0.025	0.998	0.997	0.003	0.001
	G	0.141	0.156	<0.001	<0.001	0.835	0.816	<0.001	<0.001
	POS		0.176		<0.001		0.761		<0.001
	CHROM		0.159		<0.001		0.806		<0.001
ΔPT	O3C		0.135		<0.001		0.860		<0.001
	G	0.143	0.152	<0.001	<0.001	0.808	0.796	<0.001	<0.001
	POS	0.095	0.099	<0.001	<0.001	0.940	0.931	<0.001	<0.001
	CHROM	0.143	0.155	<0.001	<0.001	0.817	0.788	<0.001	<0.001
DC	O3C	0.136	0.134	<0.001	<0.001	0.847	0.842	<0.001	<0.001
	G	0.108	0.102	<0.001	<0.001	0.948	0.931	<0.001	<0.001
	POS	0.050	0.028	<0.001	<0.001	0.979	0.993	<0.001	<0.001
	CHROM	0.125	0.133	<0.001	<0.001	0.857	0.817	<0.001	<0.001
	O3C	0.105	0.101	<0.001	<0.001	0.928	0.927	<0.001	<0.001

$n = 2240$; $n(\text{Velocity}) = 1176$.

^a This is the lower bound of real significance.

Appendix B. Correlation coefficients

Table B1. Correlations between cbPPG parameters (lines; with different color channels and ROIs) and reference O2C[®] parameters (columns) according to Bravais Pearson (*r*) and Spearman (*ρ*). Correlation strengths according to Cohen (1988) are highlighted by color and significance levels by stars (see legend).

cbPPG parameter	color channel	ROI	O2C [®] parameter							
			Flow				rHb			
			deep		surface		deep		surface	
			<i>r</i>	<i>ρ</i>	<i>r</i>	<i>ρ</i>	<i>r</i>	<i>ρ</i>	<i>r</i>	<i>ρ</i>
SNR	G	1	0.084***	0.113***	0.044*	0.065**	-0.061**	-0.046*	-0.003	0.014
		2	0.133***	0.162***	0.070**	0.097***	-0.100***	-0.083***	0.032	0.053*
	POS	1	0.123***	0.157***	0.061**	0.098***	-0.027	-0.001	0.012	0.034
		2	0.114***	0.140***	0.016	0.052*	-0.034	-0.011	-0.023	-0.003
	CHROM	1	0.048*	0.115***	-0.027	0.029	0.038	0.047*	-0.033	-0.007
		2	0.090***	0.139***	0.013	0.058**	-0.033	-0.011	0.014	0.026
	O3C	1	0.104***	0.132***	0.048*	0.084***	-0.043*	-0.016	0.000	0.016
		2	0.122***	0.150***	0.038	0.082***	-0.062**	-0.039	-0.003	0.019
logS	G	1	0.580***	0.613***	0.616***	0.677***	-0.358***	-0.358***	0.617***	0.653***
		2	0.560***	0.583***	0.605***	0.655***	-0.363***	-0.354***	0.607***	0.646***
	POS	1	-0.045*	0.014	-0.047*	0.046*	-0.102***	-0.068**	-0.011	0.021
		2	-0.045*	-0.033	0.014	0.013	-0.064**	-0.079***	0.013	0.052*
	CHROM	1	-0.097***	-0.070**	-0.099***	-0.119***	0.105***	0.074***	-0.088***	-0.052*
		2	-0.070**	-0.065**	0.048*	0.082***	-0.125***	-0.125***	-0.011	0.025
	O3C	1	0.606***	0.650***	0.680***	0.732***	-0.364***	-0.365***	0.673***	0.718***
		2	0.593***	0.617***	0.678***	0.710***	-0.382***	-0.371***	0.644***	0.681***
logN	G	1	0.521***	0.516***	0.571***	0.596***	-0.298***	-0.290***	0.527***	0.537***
		2	0.480***	0.455***	0.537***	0.532***	-0.282***	-0.269***	0.480***	0.489***
	POS	1	-0.008	0.048*	-0.018	0.080***	-0.107***	-0.048*	0.017	0.042*
		2	-0.016	-0.004	0.025	0.003	-0.060**	-0.064**	0.014	0.058**
	CHROM	1	-0.062**	-0.029	-0.086***	-0.115***	0.120***	0.080***	-0.109***	-0.065**
		2	-0.037	-0.029	0.068**	0.100***	-0.114***	-0.124***	0.004	0.033
	O3C	1	0.584***	0.596***	0.665***	0.683***	-0.323***	-0.329***	0.623***	0.653***
		2	0.558***	0.544***	0.657***	0.634***	-0.330***	-0.323***	0.585***	0.596***
ΔPT	G	1	0.698***	0.738***	0.694***	0.740***	-0.418***	-0.380***	0.664***	0.752***
		2	0.694***	0.740***	0.700***	0.750***	-0.413***	-0.389***	0.645***	0.731***
	POS	1	0.580***	0.697***	0.550***	0.637***	-0.338***	-0.250***	0.614***	0.697***
		2	0.534***	0.670***	0.535***	0.625***	-0.361***	-0.269***	0.579***	0.641***
	CHROM	1	0.634***	0.741***	0.626***	0.698***	-0.378***	-0.327***	0.634***	0.737***
		2	0.656***	0.742***	0.660***	0.718***	-0.394***	-0.362***	0.631***	0.733***
	O3C	1	0.685***	0.736***	0.640***	0.709***	-0.415***	-0.347***	0.651***	0.733***
		2	0.676***	0.732***	0.657***	0.721***	-0.422***	-0.369***	0.631***	0.699***
ampMap	G	1	0.673***	0.728***	0.669***	0.721***	-0.426***	-0.372***	0.658***	0.719***
		2	0.655***	0.714***	0.673***	0.724***	-0.414***	-0.380***	0.624***	0.684***
	POS	1	0.651***	0.706***	0.664***	0.702***	-0.403***	-0.380***	0.606***	0.684***
		2	0.624***	0.684***	0.646***	0.689***	-0.401***	-0.353***	0.599***	0.643***
	O3C	2	0.612***	0.677***	0.611***	0.679***	-0.412***	-0.362***	0.575***	0.607***
DC	G	1	-0.610***	-0.543***	-0.659***	-0.586***	0.219***	0.120***	-0.678***	-0.713***
		2	-0.566***	-0.477***	-0.614***	-0.557***	0.241***	0.191***	-0.573***	-0.585***
	POS	1	-0.017	-0.021	-0.008	-0.024	0.015	0.023	-0.019	-0.024
		2	-0.055*	-0.058**	-0.041	-0.055**	0.039	0.046*	-0.038	-0.043*
	CHROM	1	0.031	-0.005	0.055**	0.013	-0.019	0.009	0.031	0.011
		2	0.090***	0.002	0.091***	0.006	-0.014	0.042*	0.065**	0.009
	O3C	1	0.659***	0.621***	0.678***	0.627***	-0.227***	-0.156***	0.725***	0.771***
		2	0.670***	0.623***	0.736***	0.668***	-0.270***	-0.201***	0.744***	0.786***

Table B1. (Continued.)

cbPPG parameter	color channel	ROI	O2C [®] parameter							
			sO ₂				Velocity			
			deep		surface		deep		surface	
		<i>r</i>	ρ	<i>r</i>	ρ	<i>r</i>	ρ	<i>r</i>	ρ	
SNR	G	1	-0.060**	-0.034	0.078***	0.081***	-0.035	-0.038	-0.150***	-0.156***
		2	-0.050*	-0.01	0.121***	0.123***	0.016	0.021	-0.156***	-0.166***
	POS	1	-0.063	-0.041	0.060**	0.085***	-0.005	0.003	-0.151***	-0.141***
		2	-0.087***	-0.059**	0.060**	0.077***	-0.003	-0.003	-0.167***	-0.165***
	CHROM	1	-0.062**	-0.031	-0.027	0.007	-0.063*	-0.036	-0.137***	-0.105***
		2	-0.072**	-0.03	0.070**	0.087***	0.004	0	-0.166***	-0.151***
	O3C	1	-0.042*	-0.009	0.071**	0.088***	-0.032	-0.029	-0.154***	-0.154***
		2	-0.046*	-0.01	0.080***	0.098***	-0.015	-0.007	-0.166***	-0.164***
logS	G	1	0.144***	0.184***	0.617***	0.643***	0.398***	0.443***	0.207***	0.120***
		2	0.097***	0.153***	0.605***	0.627***	0.394***	0.440***	0.197***	0.101**
	POS	1	0.073**	0.079***	-0.017	0.002	0.097**	0.091**	-0.092**	-0.092**
		2	0.112***	0.075***	0.051*	0.03	-0.060*	-0.065**	0.008	-0.066*
	CHROM	1	0.049*	0.060**	-0.054*	-0.050*	-0.092**	-0.031	-0.036	0.007
		2	-0.042*	-0.001	-0.036	-0.032	-0.101**	-0.100**	0.016	-0.012
	O3C	1	0.209***	0.239***	0.643***	0.681***	0.388***	0.441***	0.261***	0.172***
		2	0.170***	0.215***	0.644***	0.667***	0.376***	0.426***	0.290***	0.184***
logN	G	1	0.096***	0.134***	0.515***	0.515***	0.371***	0.414***	0.300***	0.201***
		2	0.060**	0.109***	0.472***	0.455***	0.308***	0.347***	0.290***	0.165***
	POS	1	0.081***	0.088***	0.024	0.037	0.129***	0.106***	-0.063*	0.008
		2	0.124***	0.092***	0.063**	0.050*	-0.041	-0.034	0.019	-0.079**
	CHROM	1	0.035	0.059**	-0.068**	-0.057**	-0.132***	-0.085**	-0.025	-0.013
		2	-0.064**	-0.018	-0.041	-0.036	-0.088**	-0.082**	0.035	0.023
	O3C	1	0.189***	0.223***	0.594***	0.614***	0.372***	0.428***	0.357***	0.247***
		2	0.159***	0.194***	0.574***	0.571***	0.334***	0.383***	0.394***	0.266***
Δ PT	G	1	0.181***	0.351***	0.748***	0.833***	0.374***	0.461***	0.320***	0.167***
		2	0.171***	0.349***	0.741***	0.827***	0.365***	0.462***	0.351***	0.189***
	POS	1	0.162***	0.272***	0.735***	0.758***	0.379***	0.459***	0.121***	0.029
		2	0.154***	0.279***	0.748***	0.764***	0.367***	0.441***	0.128***	0.04
	CHROM	1	0.166***	0.301***	0.731***	0.782***	0.323***	0.450***	0.235***	0.060*
		2	0.156***	0.307***	0.736***	0.793***	0.307***	0.429***	0.294***	0.084**
	O3C	1	0.163***	0.313***	0.755***	0.805***	0.385***	0.452***	0.201***	0.084**
		2	0.154***	0.320***	0.762***	0.808***	0.376***	0.444***	0.250***	0.125***
ampMap	G	1	0.162***	0.318***	0.746***	0.812***	0.404***	0.446***	0.255***	0.141***
		2	0.138***	0.309***	0.732***	0.799***	0.390***	0.445***	0.317***	0.177***
	POS	1	0.112***	0.275***	0.709***	0.792***	0.348***	0.405***	0.318***	0.144***
		2	0.114***	0.274***	0.727***	0.775***	0.338***	0.378***	0.285***	0.120***
	CHROM	1	0.096***	0.253***	0.735***	0.754***	0.382***	0.400***	0.228***	0.124***
		2	0.096***	0.253***	0.735***	0.754***	0.382***	0.400***	0.228***	0.124***
DC	G	1	-0.194***	-0.184***	-0.585***	-0.589***	-0.327***	-0.361	-0.344***	-0.188***
		2	-0.237***	-0.229***	-0.603***	-0.587***	-0.303***	-0.345	-0.359***	-0.199***
	POS	1	0.012	-0.003	-0.04	-0.035	-0.060*	-0.026	0.071*	0.074*
		2	-0.006	-0.017	-0.064**	-0.058**	-0.091**	-0.061*	0.094**	0.088**
	CHROM	1	0.008	0.011	0.037	0.015	0.015	0.031	0.081**	0.066*
		2	-0.005	-0.008	0.055**	0.004	0.080**	0.052	0.110***	0.065*
	O3C	1	0.271***	0.275***	0.671***	0.678***	0.455***	0.486***	0.369***	0.186***
		2	0.332***	0.325***	0.717***	0.721***	0.401***	0.460***	0.411***	0.201***

● $|r| \geq 0.1$; ● $|r| \geq 0.3$; ● $|r| \geq 0.5$
 * $p < 0.05$; ** $p < 0.01$; *** $p < 0.001$
 $n = 2,240$; $n(\text{Velocity}) = 1,176$

ORCID iDs

- Alexander Hammer  <https://orcid.org/0000-0002-1984-580X>
- Matthieu Scherpf  <https://orcid.org/0000-0001-6754-5257>
- Martin Schmidt  <https://orcid.org/0000-0003-4012-0608>
- Hannes Ernst  <https://orcid.org/0000-0003-0095-8051>
- Adrian Dragu  <https://orcid.org/0000-0003-4633-2695>
- Judy Martin  <https://orcid.org/0000-0001-9898-9790>
- Olimpiu Bota  <https://orcid.org/0000-0002-5836-1269>

References

- Addison P S, Jacquelin D, Foo D M H, Antunes A and Borg U R 2017 Video-based physiologic monitoring during an acute hypoxic challenge: heart rate, respiratory rate, and oxygen saturation *Anesthesia Analgesia* **125** 860–73
- Allen J 2007 Photoplethysmography and its application in clinical physiological measurement *Physiol. Meas.* **28** R1–39
- Babchenko A, Davidson E, Ginosar Y, Kurz V, Faib I, Adler D and Nitzan M 2001 Photoplethysmographic measurement of changes in total and pulsatile tissue blood volume, following sympathetic blockade *Physiol. Meas.* **22** 389–96
- Bashkatov A N, Genina E A, Kochubey V I and Tuchin V V 2005 Optical properties of human skin, subcutaneous and mucous tissues in the wavelength range from 400 to 2000 nm *J. Phys. D: Appl. Phys.* **38** 2543–55
- Bortz J and Schuster C 2010 *Statistik für Human- und Sozialwissenschaftler* 7th edn (Berlin, Heidelberg: Springer) (<https://doi.org/10.1007/978-3-642-12770-0>)
- Bota O, Martin J, Hammer A, Scherpf M, Matschke K, Dragu A and Malberg H 2022 Topical negative pressure wound therapy enhances the local tissue perfusion—a pilot study *Microvascular Res.* **140** 104301
- Bousefsaf F, Maaoui C and Pruski A 2016 Peripheral vasomotor activity assessment using a continuous wavelet analysis on webcam photoplethysmographic signals *Bio-Med. Mater. Eng.* **27** 527–38
- Brandes R and Busse R 2011 *Kreislauf Physiologie des Menschen: mit Pathophysiologie* ed R F Schmidt, F Lang, M Heckmann et al (Berlin, Heidelberg: Springer) 572–626
- Breslow N E 1984 Extra-poisson variation in log-linear models *J. R. Stat. Soc. C* **33** 38–44
- Breslow N E and Clayton D G 1993 Approximate inference in generalized linear mixed models *J. Am. Stat. Assoc.* **88** 9–25
- Carvalho Brinca A M, de Castro Pinho A and Costa Vieira R J D 2021 Blood perfusion of random skin flaps in humans—in vivo assessment by laser speckle contrast imaging *Dermatol. Surg.* **47** 1421–6
- Clayton D and Kaldor J 1987 Empirical bayes estimates of age-standardized relative risks for use in disease mapping *Biometrics* **43** 671–81
- Cohen J 1977 *Statistical Power Analysis for the Behavioral Sciences* (New York, NY: Lawrence Erlbaum Associates) (<https://doi.org/10.1016/c2013-0-10517-x>)
- de Haan G and Jeanne V 2013 Robust pulse rate from chrominance-based rPPG *IEEE Trans. Biomed. Eng.* **60** 2878–86
- Enezi F A, Anazi A A, Mutairi M A, Shahrani M A, Qureshi S and Karthika M 2015 Arterial and venous estimation of hemoglobin: a correlational study *J. Hematol.* **4** 187–92
- Ernst H, Scherpf M, Malberg H and Schmidt M 2020 Color spaces and regions of interest in camera based heart rate estimation *2020 11th Conf. of the European Study Group on Cardiovascular Oscillations (ESGCO)* 1–2
- Ernst H, Scherpf M, Malberg H and Schmidt M 2021 Optimal color channel combination across skin tones for remote heart rate measurement in camera-based photoplethysmography *Biomed. Signal Process. Control* **68** 102644
- Fleischhauer V, Ruprecht N and Zauneder S 2019 Camera-based spatial assessment of perfusion upon stimuli *Curr. Directions Biomed. Eng.* **5** 105–8
- Francis A and Baynosa R C 2017 Hyperbaric oxygen therapy for the compromised graft or flap *Adv. Wound Care* **6** 23–32
- He Q and Wang R 2020 Hyperspectral imaging enabled by an unmodified smartphone for analyzing skin morphological features and monitoring hemodynamics *Biomed. Opt. Express* **11** 895–910
- Hertzman A B 1937 Photoelectric plethysmography of the fingers and toes in man *Proc. Soc. Exp. Biol. Med.* **37** 529–34
- Hill W F, Webb C, Monument M, McKinnon G, Hayward V and Temple-Oberle C 2020 Intraoperative near-infrared spectroscopy correlates with skin flap necrosis: a prospective cohort study *Plastic Reconstruct. Surg. Glob. Open* **8** e2742
- Holton B D, Mannapperuma K, Lesniewski P J and Thomas J C 2013 Signal recovery in imaging photoplethysmography *Physiol. Meas.* **34** 1499–511
- Huelsbusch M and Blazek V 2002 Contactless mapping of rhythmical phenomena in tissue perfusion using PPGI *Medical Imaging 2002: Physiology and Function from Multidimensional Images (SPIE Proceedings 4683)* 110–7
- Hummelink S, Kruit A S, van Vlaenderen A R W, Schreinemachers M J M, Steenbergen W and Ulrich D J O 2020 Post-operative monitoring of free flaps using a low-cost thermal camera: a pilot study *Eur. J. Plastic Surg.* **43** 589–96
- Kakashva-Mazhenkovska L, Milenkova L, Gjokik G and Janevska V 2011 Variations of the histomorphological characteristics of human skin of different body regions in subjects of different age *Prilozi* **32** 119–28
- Kamshilin A A, Miridonov S, Teplov V, Saarenheimo R and Nippolainen E 2011 Photoplethysmographic imaging of high spatial resolution *Biomed. Opt. Express* **2** 996–1006
- Kanitakis J 2002 Anatomy, histology and immunohistochemistry of normal human skin *Eur. J. Dermatol.* **12** 390–401
- Kohlert S, Quimby A E, Saman M and Ducic Y 2019 Postoperative free-flap monitoring techniques *Semin. Plastic Surg.* **33** 13–6
- Koo T K and Li M Y 2016 A guideline of selecting and reporting intraclass correlation coefficients for Reliability Research *J. Chiropractic Med.* **15** 155–63
- Krug A 2006 Mikrozirkulation und sauerstoffversorgung des gewebes *Phlebologie* **35** 300–12
- Kyriacou P A, Zaman T and Pal S K 2020 Photoplethysmography in postoperative monitoring of deep inferior epigastric perforator (DIEP) free flaps *Physiol. Meas.* **41** 124001
- Marcinkevics Z, Rubins U, Zaharans J, Urtane A M M d E and Ozolina-Moll L 2016 Imaging photoplethysmography for clinical assessment of cutaneous microcirculation at two different depths *J. Biomed. Opt.* **21** 035005
- McDuff D and Blackford E 2019 iPhys: An Open Non-Contact Imaging-Based Physiological Measurement Toolbox *2019 41st Annual International Conference of the IEEE Engineering in Medicine and Biology Society (EMBC)* 6521–4 arXiv:1901.04366
- Mishra D, Priyadarshini N, Chakraborty S and Sarkar M 2017 Blood oxygen saturation measurement using polarization-dependent optical sectioning *IEEE Sens. J.* **17** 3900–8
- Muenchow S, Horch R E and Dragu A 2019 Effects of topical negative pressure therapy on perfusion and microcirculation of human skin *Clin. Hemorheol. Microcirc.* **72** 365–74
- Nitzan M, de Boer H, Turivnenko S, Babchenko A and Sapoznikov D 1994 Power spectrum analysis of spontaneous fluctuations in the photoplethysmographic signal *J. Basic Clin. Physiol. Pharmacol.* **5** 269–76
- Patel U A et al 2017 Free flap reconstruction monitoring techniques and frequency in the era of restricted resident work hours *JAMA Otolaryngol.—Head Neck Surg.* **143** 803–9
- Rahmanian-Schwarz A, Rothenberger J, Amr A, Jaminet P and Schaller H-E 2012 A postoperative analysis of perfusion dynamics in deep inferior epigastric perforator flap breast reconstruction: a noninvasive quantitative measurement of flap oxygen saturation and blood flow *Ann. Plast. Surg.* **69** 535–9
- Rasche S, Huhle R, Junghans E, de Abreu M G, Ling Y, Trumpp A and Zauneder S 2020 Association of remote imaging photoplethysmography and cutaneous perfusion in volunteers *Sci. Rep.* **10** 16464

- Reisner A, Shaltis P A, McCombie D, Asada H H, Warner D S and Warner M A 2008 Utility of the photoplethysmogram in circulatory monitoring *Anesthesiology* **108** 950–8
- Secerbegovic A, Mesic H, Bergsland J and Balasingham I 2019 Contactless blood perfusion assessment of the free flap in breast reconstruction surgery 2019 13th International Symposium on Medical Information and Communication Technology (ISMICT) 1–4
- Song Y-G, Chen G-Z and Song Y-L 1984 The free thigh flap: a new free flap concept based on the septocutaneous artery *Br. J. Plastic Surg.* **37** 149–59
- Sun J M, Chew K Y, Wong C H and Goh T L H 2017 Vascular anatomy of the anteromedial thigh flap *JPRAS Open* **13** 113–25
- Trumpp A 2019 Remote assessment of the cardiovascular function using camera-based photoplethysmography *Doctoral Thesis Technische Universität Dresden, Dresden* <https://nbn-resolving.org/urn:nbn:de:bsz:14-qucosa2-367589>
- Trumpp A, Schell J, Malberg H and Zauneder S 2016 Vasomotor assessment by camera-based photoplethysmography *Curr. Directions Biomed. Eng.* **2** 199–202
- Tsouri G R and Li Z 2015 On the benefits of alternative color spaces for noncontact heart rate measurements using standard red-green-blue cameras *J. Biomed. Opt.* **20** 048002
- Verkruyse W, Bartula M, Bresch E, Rocque M, Meftah M and Kirenko I 2017 Calibration of contactless pulse oximetry *Anesthesia Analgesia* **124** 136–45
- Verkruyse W, Svaasand L O and Nelson J S 2008 Remote plethysmographic imaging using ambient light *Opt. Express* **16** 21434–45
- Wang W, den Brinker A C, Stuijk S and de Haan G 2017 Algorithmic principles of remote PPG *IEEE Trans. Biomed. Eng.* **64** 1479–91
- Williams D A 1982 Extra-binomial variation in logistic linear models *J. R. Stat. Soc. C* **31** 144–8
- Wu T, Blazek V and Schmitt H J 2000 Photoplethysmography imaging: a new noninvasive and noncontact method for mapping of the dermal perfusion changes *EOS/SPIE EUROPEAN BIOMEDICAL OPTICS WEEK: Optical Techniques and Instrumentation for the Measurement of Blood Composition, Structure, and Dynamics 1 (SPIE Proceedings 4163)* 62–70
- Yang J, Guthier B and El Saddik A 2015 Estimating two-dimensional blood flow velocities from videos 2015 IEEE Int. Conf. on Image Processing (ICIP) 3768–72
- Zauneder S, Trumpp A, Wedekind D and Malberg H 2018 Cardiovascular assessment by imaging photoplethysmography—a review *Biomed. Eng./Biomedizinische Technik* **63** 617–34
- Zauneder S, Trumpp A, Ernst H, Förster M and Malberg H 2018 Spatio-temporal analysis of blood perfusion by imaging photoplethysmography *Optical Diagnostics and Sensing XVIII: Toward Point-of-Care Diagnostics (SPIE Proceedings 10501)* 105010X